ASME Paper Title:

A comparison of characteristics of periodic surface micro/nano structures generated via single laser beam direct writing and particle lens array parallel beam processing

Authors: Fatema H. Rajab
Anmar K. Al-Jumaily
Tayf Tariq A.S.
Sorin Laurentiu Stanescu
Ahmad W. AlShaer
Lin Li
Rwayda Kh. S. Al-Hamd

ASME Journal Title: Journal of Micro and Nano-Manufacturing

Volume/Issue 9/2

Date of Publication (VOR* Online) 15 September 2021

ASME Digital Collection URL: https://asmedigitalcollection.asme.org/micronanomanufacturing/article/9/2/021007/1115768/A-Comparison-of-Characteristics-of-Periodic

DOI: https://doi.org/10.1115/1.4052140

A Comparison of Characteristics of Periodic Surface Micro/Nano Structures Generated Via Single Laser Beam Direct Writing and Particle Lens Array Parallel Beam Processing

Fatema H. Rajab[1]
Laser and Optoelectronics Engineering Department,
College of Engineering,
Al-Nahrain University,
Baghdad, Iraq
E-mail: fatema.h.rajab@nahrainuniv.edu.iq, fatema.hamid.rajab@gmail.com

Anmar K. Al-Jumaily
Laser and Optoelectronics Engineering Department,
College of Engineering,
Al-Nahrain University,
Baghdad, Iraq

Tayf Tariq A.S
University of Information Technology and Communications,
Baghdad, Iraq

Sorin Laurentiu Stanescu
LIG Nanowise Ltd, Unit 15, Williams House, Manchester Science Park
Pencroft Way, M15 6SE, Manchester

Ahmad W. AlShaer
School of Engineering,
University of Central Lancashire (UCLan),
Preston, UK

Lin Li
Laser Processing Research Centre,
Department of Mechanical, Aerospace, and Civil Engineering,
The University of Manchester,
Manchester, M13 9PL, UK

Rwayda Kh. S. Al-Hamd

School of Applied Sciences,
Abertay University,
Dundee, UK

[1] Corresponding Author

ABSTRACT

Changing material surface micro/nano structures using laser beam texturing is a valuable approach in wide applications such as control of cell/bacterial adhesion and proliferation, solar cells and optical metamaterials. Here we report a comparison of the characteristics of surface micro/nano structures produced using single beam laser direct writing and particle lens array parallel laser beam patterning. A Nd:YVO_4 nanosecond pulsed laser at 532 nm wavelength was used in the laser direct writing method to texture the stainless steel surface submerged in water and in air with different scanning patterns. Changes in surface morphology, wettability, surface chemistry and optical reflectivity were analyzed. In the particle lens array method, an excimer nanosecond laser at 248 nm wavelength was adopted to produce surface patterns on GeSbTe (GST) film coated on a polycarbonate substrate by splitting and focusing a single laser beam into millions of parallel breams. Single beam laser direct writing shows that the surface of high roughness and oxygen percentage content presented high wettability and low reflectivity characteristics. However, the controllability of the type of surface micro/nano patterns is limited. The parallel laser beam processing using particle lens array allows rapid production of user designed periodic surface patterns at nano-scale overcoming the optical diffraction limit with a high degree of controllability. Controlling the uniformity of the particle lens array is a challenge.

Keywords: *Laser; surface texture; structure; micro; nano; pattern; microsphere; parallel; morphology; wettability; reflectivity; and particle lens array.*

1. INTRODUCTION

Modifying surface properties by producing tailored nano/microstructures have been extensively died and has found wide applications in several fields including self-cleaning, coating adhesion, wear resistance, anti-icing, and biological applications. Moreover, changing the surface optical properties is used for solar cell and photoresist applications [1–8]. Many surface engineering methods are available to modify the surface structures, including chemical etching, sandblasting, mechanical machining, corona discharge, plasma etching, and laser surface texturing. Among these techniques, laser surface texturing is one of the most efficient and flexible techniques. It has been used to produce smart surfaces that meet the requirements for more stringent surface structure designs and properties. Besides, laser surface texturing has the advantages of fast processing speed, non-contact processing, ease for automation, zero tool wear, and non-dross ablation [9,10].

Different techniques have been used in laser surface texturing for producing different structures, including laser direct writing with or without using a mask, two or multi-beam interference and particle lens array multiple laser beam patterning [11]. According to the surface feature size, laser surface texturing can be classified as micro-scale, nano-scale, or multi-scale surfaces (hierarchal structures, with a combination of micro/nano features). Various structures such as holes, grooves, bumps, protrusions, periodic surface structures, spikes, conic structures have been produced using laser direct writing [9,12,13]. The generation of various types of surface patterns depends mainly on the laser parameters, such as including fluence/power density, wavelength,

pulse duration, scanning speed, and the number of pulses; processing environment; and material parameters. These parameters' relationship affects the generated surface properties and quality [9,13,14].

For micro/nano structuring, short and ultrashort lasers have been used using laser direct writing method. The laser surface texturing process using ultrashort lasers is mainly due to vaporization and plasma formation, while melting, splashing, and solidification dominate the process of laser surface texturing using short pulse duration like nanosecond laser. Using a nanosecond laser, high throughput can be achieved compared to ultrashort laser processing due to the high laser fluence of melting and solidification [15,16].

The laser surface structuring technique using contact particle lens array is a near-field technique in which the microspheres are deposited on the substrate, forming a self-assembled monolayer on the substrate. These microspheres behave as lenses splitting and focusing a single laser beam to many beams on the substrate, and each spot generates tailored features forming periodic nano-scale surface structures. Implementing this technique, it is possible achieve features with a resolution down to $\lambda/3$ [11,17]. Different techniques have been used for microsphere deposition including dip coating, spin coating, and convective coating. The convective coating has been the most commonly used technique. The efficiency of the monolayer microsphere lens array depends on the capillary force between particles and the adhesion force in which the monolayer adheres to the substrate. Various nano-features such as star, bumps, holes, and grooves have been generated using particle lens array laser patterning [18–20].

This work was motivated by the practical engineering challenges of producing surfaces with various micro and nanostructures using flexible and efficient ways. Therefore, in this paper, two laser surface texturing techniques are compared to examine the properties of surfaces with various structures and properties. The first technique is the laser direct writing. This process is performed using nanosecond laser processing of a stainless steel surface to modify the surface structure and properties. The second technique is the contact particle lens array used to generate micro/ nanostructures on a thin film of GeSbTe (GST) film coated on a polycarbonate substrate.

2. EXPERIMENTAL PROCEDURE

For the laser direct writing method, AISI 316L stainless steel sheets were used in this work. These sheets were cut to the dimensions of 10 mm x 10 mm x 0.7 mm. Before the laser treatment, the sheets were cleaned ultrasonically using acetone, ethanol, and di-ionized water, for 10 minutes each and dried used compressed air.

A Nd:YVO_4, nanosecond laser (Laserline Laserval Violino) was selected to study the effect of laser processing parameters such as scanning speed and hatch distances on micro structuring wettability, reflectivity and oxygen surface content. The effect of scanning direction, laser fluence, laser scanning speed and scanning environment on the surface morphology were examined. The laser beam was directed using a set of x-y Galvo scanning mirrors and an F-theta lens. In some experiments, the sample was submerged in water in order to reduce surface oxidation and reduce the feature sizes and compared that processed in air. The level of water for the submerged sample experiments was 1 mm above the sample. The laser scanning was performed in one

direction, two or more directions. The effect of scanning direction on the surface morphology was studied. The experimental scheme is shown in Fig. 1. Table 1 listed the laser processing parameters used in this work.

Prior to the surface characterization after laser treatment, the samples were ultrasonically cleaned using Ethanol then compressed air to remove any ablated materials and contamination. Scanning electron microscopy (Philips XL30 FEG-SEM) was used to examine the surface morphology. This SEM is combined with energy dispersive X-ray (EDX) which was used to characterize the surface oxygen contents. A confocal laser scanning microscope (type: Keyence 3D profiler) was used to examine the surface roughness. Water drops sessile method using a contact angle analyzer (type: FTA 188) was used to investigate laser textured surfaces' wettability characteristics. In this method, a contact angle of 10 µl droplets of de-ionized water that contact the surface was measured.

For particle lens array experiment, GeSbTe (GST) film coated on a polycarbonate substrate was used in this work. GeSbTe is a composite of three materials (germanium-antimony-tellurium or GST) and it is a phase-change material from the group of chalcogenide glasses used in rewritable optical discs and phase-change memory applications. The crystallization temperature of this alloy is between 100 and 150 °C, and its melting point is around 600 °C. It is characterized as a high speed phase change material and its crystallization time around 20 nanoseconds which make it easy for patterning. The reason for the selection of this material is because it requires very low laser energy density to cause surface morphology change, ideal for the particle lens

surface patterning applications. The sample was a 20 nm thick Germanium-Antimony-Tellurium (GST) film coated on a polycarbonate substrate. A low concentration of 4.74 μm SiO_2 microspheres was prepared by buffering the microspheres solution in de-ionized water. The solution was spread over the substrate to form a monolayer. Then the water evaporated when the samples were placed with a 90° angle.

A KrF Excimer laser (GSI-Lumonic IPEX848) was used to irradiate the samples using the setup shown in Fig. 2. The laser beam size was 25×25 mm with a uniform intensity distribution and a lens (focal length = 10 mm) was used to focus the laser on the sample with a spot area 10 mm × 10 mm. the laser processing parameters are listed in Table 2. For imaging the microsphere morphology formed on a film substrate and nano patterns generated after laser irradiation, optical microscopy (type: Leica CH-9435) was used.

3. RESULTS AND DISCUSSION

3.1 Laser direct writing

3.1.1 Surface morphology

Figures 3-6 show different scanning techniques that have been conducted in this work. Various and homogeneous structures ranging from ripples to porous and conical structures were achieved by changing the scanning directions, scanning speed, laser fluence, and processing environment. Figure 3 shows the nanosecond laser surface texturing's typical surface morphology using five different scanning patterns. It can be seen that by changing the angle of scanning from (0˚, 90˚) to (10˚, 130˚), (0˚,90˚,45˚, -45˚), and (10˚, 130˚), the surface morphology was changed from conical like structure to micro-pores, beehive, and diamond-like structures, respectively. The scanning was

182 performed at a 100 mm/s scanning speed, a 50 µm hatch distance, a 7 ns pulse
183 duration, a 30 kHz pulse repetition rate, a 3.9 J/cm² laser fluence and 10 repeat scanning
184 passes.

185 The effect of laser scanning speed on the microstructure morphology was also
186 studied (Fig. 4). The scanning was performed using one direction scanning and laser
187 parameters of (9.8 J/cm² laser fluence, one pass, and 50 µm hatch distance). It can be
188 seen that changing the scanning speed from 2000 mm/s to 1 mm/s changed the
189 microstructure from an oval-like structure to a cauliflower-like structure.

190 Figure 5 shows the microstructure of surfaces generated using three laser
191 fluences. The scanning was performed using two directions (30˚ and 60˚), using laser
192 parameters of (100 mm/s scanning speed, 50 µm hatch distance and 10 times passes). It
193 can be seen that micro ripples were formed using low laser fluence (0.9 J/cm²) (Fig. 5a),
194 while it changed to a hierarchal microstructure using a high laser fluence (9.8 J/cm²)
195 (Fig. 5c).

196 Figure 6 shows the difference between the microstructures generated in water
197 and air. Using laser parameters of (9.8 J/cm², 10 mm/s scanning speed, 25 µm hatch
198 distance, and 1 pass), the microstructure in the air was cauliflower likes structure, while,
199 in water, a uniform conical like structure was formed.

200 Changing the scanning direction and scanning speeds affects the number of
201 pulses and the laser overlapping which in turn affected the surface structure. The pulse
202 overlapping can be calculated as [9,21]:

203 $$\left(1 - \frac{\Delta x}{spot\ size}\right) \times 100 \qquad (1)$$

The line overlapping can be calculated as [9,21]:

$$(1 - \frac{\Delta z}{spot\ size}) \times 100 \qquad (2)$$

Where, $\Delta x = \frac{speed}{repetition\ rate}$ and Δz is the hatch distance.

In this work, the line overlapping was 81.8 %, and the pulse overlapping was 39 % and 99.9 % at 1000 mm/s and 1 mm/s laser speeds, respectively. The number of pulses per spot can be estimated as $\frac{Spot\ size * repetition\ rate}{scanning\ speed}$, and it was 2 and 1650 at a laser speed of 1000 mm/s and 1 mm/s, respectively.

By increasing the laser fluence from 0.9 J/cm² to 9.8 J/cm², the surface microstructure changed from micro ripples to a 3D complex structure. This is related to the increase the material removal by increasing the laser fluence. The removed materials could be solidified around the laser scanning area forming complicated 3D structures [22].

By changing the laser-processing environment from air to water, the microstructure was changed to be smooth and free of solidified material and particles over the microstructure. The reason behind this is that the ablated particles were moved with water movement and they did not redeposit over the surface during laser processing of the material in water [9,23,24].

3.1.2 Surface characteristics

The surface roughness (Ra) measurements of as-received surface (control) were 10.9±3.54 nm. Figure 7 shows the roughness values of laser treated surfaces using a range of scanning speeds and hatch distances. It is clear that the surface roughness was

proportional to the hatch distances and inversely proportional to the laser scanning speed. The surface generated using a hatch distance of 100 μm and a scanning speed of 10 mm/s recorded the highest surface roughness Ra value (11.12 ± 1.8 μm) compared to those of other surfaces. Surface generated using a 10 μm hatch distance and a 1000 mm/s scanning speed, on the other hand, showed the smallest surface roughness (0.12 ± 0.007 μm) compared to other surfaces.

Figure 8 shows the analysis data of the energy-dispersive X-ray spectroscopy (EDXs) for surfaces. As received surface (control) was free of oxidation as its' measured oxygen percentage was zero. However, after laser processing, it was noticed that the surface oxygen content of all processed samples was increased. By increasing the laser scanning speed and the hatch distance, the oxygen percentage decreased. For example, at a speed of 10 mm/s, the oxygen percentage recorded 21.8 % and 7.8 % using, respectively, 10 μm and 100 μm hatch distances. However, at a speed of 1000 mm/s, the oxygen percentage was 0.93 % at 10 μm hatch distance and less than 0.4 % using 100 μm hatch distance.

In this work, the effect of ns laser generated surface structures on the change of the stainless steel (SS) wettability was investigated. The contact angle of as received substrate (control) was 90.5˚±3.5˚. After laser treatment, all the surfaces performed superhydrophilic properties with a contact angle CA=0˚ immediately after the laser processing. However, the wettability characteristics of all processed samples changed with time. Therefore, the contact angle was measured again at one month after laser processing. Figure 9 shows the surface wettability change as a function of the laser

scanning speed and hatch distances. It is clear that the contact angle increased with increasing scanning speed and hatch distance. The surface produced at a 1000 mm/s and 100 μm hatch distance was superhydrophobic with maximum contact angles (CAs) around 158°. However, the minimum CA was ~ 125° for the surface generated at a 10 mm/s scanning speed and 10 μm hatch distance. Generally, the wettability of surfaces was inversely proportional to the scanning speed and hatch distance.

Figures 10 and 11 show the change of surface reflectivity within the visible light spectrum (400 – 700 nm) after the laser processing. The reflectivity was investigated for samples treated using different laser speeds and hatch distances. It can be seen that the reflectivity of all processed surfaces was decreased compared to the reflectivity of as received substrate (control) (Fig. 10). Furthermore, at a specific hatch distance, it can be seen that the reflectivity of surfaces was increased with increasing the scanning speed (Fig. 10). Moreover, at a specific scanning speed, the results show that the reflectivity of laser-treated surfaces was increased with increasing hatch distance (Fig. 11). The reflectivity of as received stainless steel (control) was about 60 %. However, the reflectivity was decreased to less than 2 % for samples treated using 10 mm/s laser speed and 10 μm hatch distance.

In this work, it was observed that laser processing parameters affected the surface properties. Changing the surface characteristics with changing the laser processing parameters has been extensively studied before. Some researchers have reported that the surface wettability increases with increasing the surface oxygen contents and surface roughness [25] . With increasing surface roughness, the contact

area between the surface and water droplets increased due to the natural gravitational desire to settle on the surface [26,27]. Cui et al. [28] reported that heating the stainless steel increased the oxygen contents from the surrounding environment forming Fe_2O_3 and Cr_2O_3. The hydroxyl group (OH density) increased the surface oxygen contents, thereby increasing the surface adsorption and surface wettability [26,27]. In our work, during material processing, it was noticed that the surface reflectivity was decreased, and some surfaces switched to black. Other researchers also noticed this behavior during different processing materials such as Si [29]. This is related to increasing the surface roughness, which leads to increased surface area and multiple reflections inside the surface features [9,30].

3.2 Particle lens array parallel laser beam surface patterning

Parallel processing techniques are essential to generate micro/nano-textures over a large area. Particle lens arrays can be used to produce micro and nanostructures by splitting a single laser beam into millions or billions of laser beams and focusing locally without diffraction limit. This technique is based on near-field effect of small transparent microspheres to produce micro/nano-patterns. Using this technique, it is possible to produce a feature size below the diffraction limit. Monodispersed 4.74 μm spherical silica (SiO_2, Duke Scientific) particles were diluted with de-ionized water and applied to the film surface. After the water evaporated, a hexagonally closed-packed monolayer was formed on the surface due to the self-assembly process. The sample was then laser processed and characterized using a Leica CH-9435 microscope (Fig. 12).

Normal incidence of a laser beam onto the substrate surface removes most of the particles (spheres) from the substrate after a single laser pulse irradiation. The disappearance of the particles makes it impossible to fabricate arbitrary shaped patterns. To keep particles on the substrate surface for multiple pulses processing, an angled beam scanning technique was used and a software tool was developed using this principle. As the incident angle increases, a higher percentage of the particles are left on the sample surface. This effect is because the ablation point is not located at the contacting point of the particle and the substrate. With the developed technique, different user defined nanostructures have been produced by a certain number of laser pulses. Virtually, millions of parallel features like lines, curves and even more complex profiles could be written simultaneously over large surface areas. Patterns of a complex shape were created on the substrate surface using software developed in Matlab 2010b (32 bits edition), which is a powerful programming environment for professional scientific and engineering applications. The software is compatible to all the Newport Motion Controllers/Drivers (due to their common commands and answers) and can be easily adjusted for other motion control systems and lasers according to the forward documentation.

User-defined complex shapes can be fabricated within regions $d_p \leq r$, as shown in Fig. 13. The position of ablation spot p(α, ϕ) is a function of the incident angle α and sample rotating angle φ. Angle α controls the position of *p i*n radial direction, while angle φ moves *p* in circumferential direction. The ranges of angles are α(-45°, 0°) and ϕ(-

311 180° , 180°). By applying a relative angle *α(φ)* with every rotated angle *φ*, user-defined
312 patterns can be easily fabricated.

313 According to the Mie theory, the induced near-field enhancement is located
314 around the particle and along to incident direction. It is known that the enhanced
315 intensity will decay along the incident direction before it reaches the substrate surface.
316 If the laser energy is sufficient, this enhanced field is still able to ablate materials for the
317 substrate surface. The shift of these peak positions away from the contact point with a
318 distance close to that is given by the geometrical optics:

319 $$d_p \cong r \cdot \tan(\alpha) \qquad (3)$$

320 where *r* is the radius of the particle.

321 Figures 14 and 15 show two periodic patterns generated on the GeSbTe film
322 using an excimer laser. Figures 14a and 15a show the computer design of a square
323 shape and (nano) in the software interface, which led to the patterning of the GeSbTe
324 (GST) film with uniform periodic patterns. The gaps between dots cannot be
325 distinguished due to their overlapping (one can see in Figs. 14a and 15a) and of melting
326 of the film during the laser processing. The fluence used was 1 mJ/cm^2. The experiments
327 were performed with two Newport PR 50 Series computer-controlled rotation stages
328 and a Newport ESP300 controller. One stage controls the laser incident angle *α* by tilting
329 the sample with angles ranged from 0° to 45°. The other stage rotates the sample within
330 the tilted plane with an angle ϕ with angles ranged from -180° to 180°. Therefore, any
331 point p (α, ϕ) within the shade of particle on the substrate surface could be reached by
332 a geometrical calculation of angles *α* and *φ*.

The developed technique could provide means to produce arbitrary patterned surfaces on small objects such as MEMS (for improved tribological characteristics), OLEDs (for improved emission efficiency), optical metamaterials, uniform structures for cell and bacterial adhesion and migration, and medium-sized objects.

In this work, the results showed that the surface properties and structure could be controlled by controlling the processing method. Using laser direct writing method, the results showed that increasing the surface wettability and absorptivity were related to increasing the surface roughness and oxygen percentage content. However, the controllability of the type of surface micro/nano patterns is limited. The parallel laser beam processing using a particle lens array, on the other hand, allowed rapid production of user-designed periodic surface patterns at nano-scale, overcoming the optical diffraction limit with a high degree of controllability where controlling the uniformity of the particle lens array is a challenge.

4. CONCLUSION

In this work, nanosecond pulsed lasers were used to generate different micro/nanostructures using two different techniques: direct writing and particle lens array parallel writing. In the laser direct writing technique, the substrate was melted and evaporated, and then the re-deposition and solidification of molten materials generated different microstructures. Therefore, the formation of different structures using the ns laser was mainly due to the thermal effects on treated surfaces. The surface morphology and properties were changed with changing laser-processing parameters. Moreover, the surfaces processed a low scanning speed (10 mm/s) recorded the highest roughness and oxygen percentage content and the minimal wettability and reflectivity

compared to other surfaces. Furthermore, the surfaces produced at 100 µm recorded the highest roughness, water contact angle and reflectivity and minimal oxygen percentage contents compared to other surfaces generated using 10 µm and 50 µm hatch distances. Thus, the surface of high roughness and oxygen percentage content presented a high wettability and turned to black with low reflectivity characteristics. Using particle lens array technique, two nano-patterns were demonstrated. This is a very efficient way of producing tailored surface micro/nano patterns. Both processing methods presented effective surfaces. This study shows that nanosecond lasers could generate distinctive morphologies and properties using easy and efficient ways. These surfaces could be useful in various applications, including biological applications, wear resistance, self-cleaning, anti-icing, coating adhesion, and solar cells.

Acknowledgments

The authors thank The University of Manchester, especially Professor Lin Li for facilitating conducting this work in their laboratories.

REFERENCES

[1] Hsu, S.-T., Wang, H., Satoh, G., and Yao, Y. L., 2011, "Applications of Surface Structuring with Lasers," *International Congress on Applications of Lasers & Electro-Optics*, Laser Institute of America, pp. 1095–1104.

[2] Zhang, L., Zhao, N., and Xu, J., 2014, "Fabrication and Application of Superhydrophilic Surfaces: A Review," J. Adhes. Sci. Technol., **28**(8–9), pp. 769–790.

[3] Byon, C., Nam, Y., Kim, S. J., and Ju, Y. S., 2010, "Drag Reduction in Stokes Flows over Spheres with Nanostructured Superhydrophilic Surfaces."

[4] Rajab, F. H., Liauw, C. M., Benson, P. S., Li, L., and Whitehead, K. A., 2018, "Picosecond Laser Treatment Production of Hierarchical Structured Stainless Steel to Reduce Bacterial Fouling," Food Bioprod. Process., **109**.

[5] Rajab, F. H., Liauw, C. M., Benson, P. S., Li, L., and Whitehead, K. A., 2017, "Production of Hybrid Macro/Micro/Nano Surface Structures on Ti6Al4V Surfaces by Picosecond Laser Surface Texturing and Their Antifouling Characteristics," Colloids Surfaces B Biointerfaces, **160**.

[6] Rajab, F. H., Liu, Z., Wang, T., and Li, L., 2019, "Controlling Bacteria Retention on Polymer via Replication of Laser Micro/Nano Textured Metal Mould," Opt. Laser Technol., **111**(May 2018), pp. 530–536.

[7] Rajab, F. H., Korshed, P., Liu, Z., Wang, T., and Li, L., 2019, "How Did the Structural ZnO Nanowire as Antibacterial Coatings Control the Switchable Wettability," Appl. Surf. Sci., **469**(June

2018), pp. 593–606.
[8] Buividas, R., Stoddart, P. R., and Juodkazis, S., 2012, "Laser Fabricated Ripple Substrates for Surface-enhanced Raman Scattering," Ann. Phys., **524**(11), pp. L5–L10.
[9] Rajab, F. H., Whitehead, D., Liu, Z., and Li, L., 2017, "Characteristics of Hierarchical Micro/Nano Surface Structure Formation Generated by Picosecond Laser Processing in Water and Air," Appl. Phys. B Lasers Opt., **123**(12).
[10] Guan, Y. C., Luo, F. F., Lim, G. C., Hong, M. H., Zheng, H. Y., and Qi, B., 2015, "Fabrication of Metallic Surfaces with Long-Term Superhydrophilic Property Using One-Stop Laser Method," Mater. Des., **78**, pp. 19–24.
[11] Bäuerle, D., 2013, *Laser Processing and Chemistry*, Springer Science & Business Media.
[12] Ahmmed, K. M., Grambow, C., and Kietzig, A.-M., 2014, "Fabrication of Micro/Nano Structures on Metals by Femtosecond Laser Micromachining," Micromachines, **5**(4), pp. 1219–1253.
[13] Rajab, F. H., Liu, Z., and Li, L., 2018, "Production of Stable Superhydrophilic Surfaces on 316L Steel by Simultaneous Laser Texturing and SiO<inf>2</Inf>deposition," Appl. Surf. Sci., **427**.
[14] William, M. S., and Mazumder, J., 2010, "Laser Material Processing," Steen springer-Verlag, London, Berlin, Heidelb., **3**, p. 408.
[15] Cunha, A., Zouani, O. F., Plawinski, L., Botelho do Rego, A. M., Almeida, A., Vilar, R., and Durrieu, M.-C., 2015, "Human Mesenchymal Stem Cell Behavior on Femtosecond Laser-Textured Ti-6Al-4V Surfaces," Nanomedicine, **10**(5), pp. 725–739.
[16] Perni, S., and Prokopovich, P., 2013, "Micropatterning with Conical Features Can Control Bacterial Adhesion on Silicone," Soft Matter, **9**(6), pp. 1844–1851.
[17] Khan, A., Wang, Z., Sheikh, M. A., Whitehead, D. J., and Li, L., 2011, "Laser Micro/Nano Patterning of Hydrophobic Surface by Contact Particle Lens Array," Appl. Surf. Sci., **258**(2), pp. 774–779.
[18] Khan, A., Wang, Z., Sheikh, M. A., Whitehead, D. J., and Li, L., 2010, "Parallel Near-Field Optical Micro/Nanopatterning on Curved Surfaces by Transported Micro-Particle Lens Arrays," J. Phys. D. Appl. Phys., **43**(30), p. 305302.
[19] Guo, W., Wang, Z. B., Li, L., Whitehead, D. J., Luk'yanchuk, B. S., and Liu, Z., 2007, "Near-Field Laser Parallel Nanofabrication of Arbitrary-Shaped Patterns," Appl. Phys. Lett., **90**(24), p. 243101.
[20] Li, L., Guo, W., Wang, Z. B., Liu, Z., Whitehead, D., and Luk'yanchuk, B., 2009, "Large-Area Laser Nano-Texturing with User-Defined Patterns," J. Micromechanics Microengineering, **19**(5), p. 54002.
[21] Lehr, J., and Kietzig, A.-M., 2014, "Production of Homogenous Micro-Structures by Femtosecond Laser Micro-Machining," Opt. Lasers Eng., **57**, pp. 121–129.
[22] Harimkar, S. P., and Dahotre, N. B., 2006, "Effect of Laser Fluence on Surface Microstructure of Alumina Ceramic," Adv. Appl. Ceram., **105**(6), pp. 304–308.
[23] Razi, S., Madanipour, K., and Mollabashi, M., 2016, "Laser Surface Texturing of 316L Stainless Steel in Air and Water: A Method for Increasing Hydrophilicity via Direct Creation of Microstructures," Opt. Laser Technol., **80**, pp. 237–246.
[24] Daminelli, G., Krüger, J., and Kautek, W., 2004, "Femtosecond Laser Interaction with Silicon under Water Confinement," Thin Solid Films, **467**(1–2), pp. 334–341.
[25] Razi, S., Madanipour, K., and Mollabashi, M., 2015, "Improving the Hydrophilicity of Metallic Surfaces by Nanosecond Pulsed Laser Surface Modification," J. Laser Appl., **27**(4), p. 42006.
[26] Takeda, S., Fukawa, M., Hayashi, Y., and Matsumoto, K., 1999, "Surface OH Group Governing Adsorption Properties of Metal Oxide Films," Thin Solid Films, **339**(1–2), pp. 220–224.
[27] Takeda, S., and Fukawa, M., 2003, "Surface OH Groups Governing Surface Chemical Properties of SiO2 Thin Films Deposited by RF Magnetron Sputtering," Thin Solid Films, **444**(1–2), pp. 153–157.
[28] Cui, C. Y., Cui, X. G., Ren, X. D., Qi, M. J., Hu, J. D., and Wang, Y. M., 2014, "Surface Oxidation Phenomenon and Mechanism of AISI 304 Stainless Steel Induced by Nd: YAG Pulsed Laser," Appl. Surf. Sci., **305**, pp. 817–824.
[29] Vorobyev, A. Y., and Guo, C., 2011, "Direct Creation of Black Silicon Using Femtosecond Laser Pulses," Appl. Surf. Sci., **257**(16), pp. 7291–7294.
[30] Ta, D. V, Dunn, A., Wasley, T. J., Kay, R. W., Stringer, J., Smith, P. J., Connaughton, C., and Shephard, J. D., 2015, "Nanosecond Laser Textured Superhydrophobic Metallic Surfaces and Their Chemical Sensing Applications," Appl. Surf. Sci., **357**, pp. 248–254.

499 **Figure Captions List**
500

Fig. 1 (a) Experimental set up and (b) scanning directions with: (b1) one direction scanning, (b2) two directions scanning, (b3) four directions scanning, (b4) two directions with 30° & 60° scanning and (b5) two directions with 10° & 130° scanning

Fig. 2 Experimental set up of surface texturing using particle lens array

Fig. 3 Effect of the scanning direction on the microstructure morphology: (a) conical, (b) micro-pores, (c) beehive and (d) diamond-like structures.

Fig. 4 Effect of scanning speed on the microstructure morphology using: (a) 2000 mm/s, (b) 500 mm/s, (c) 100 mm/s and (d) 1 mm/s. Scale bar is 200 µm

Fig. 5 Effect of laser fluence on the microstructure morphology using: (a) 0.9 J/cm², (b) 3.9 J/cm², and (c) 9.8 J/cm²

Fig. 6 The microstructure morphology generated in: (a) water, and (b) air, the scale bar is 50 µm

Fig. 7 The surface roughness measurements of laser treated surfaces

Fig. 8 The surface oxygen contents measurements of laser treated surfaces

Fig. 9 The contact angle measurements of laser treated surfaces

Fig. 10 The surface reflectivity measurements of laser treated surfaces

Fig. 11 The surface reflectivity measurements as a function of changing hatch distances at a scanning speed of 10 mm/s

Fig. 12 Optical microscope image of a uniform layer of SiO_2 microsphere using: (a) 10X magnification and (c) 20X magnification

Fig. 13 Schematic diagram of geometric algorithm between the position of spot p, incident angle α and sample rotating angle ϕ

Fig. 14 a. Matlab® software interface; b. 2D generated square micro-patterns onto a GeSbTe film using a laser fluence of 1mJ/cm^2 and 4.74 μm diameter SiO_2 microspheres

Fig. 15 a. Matlab® software interface; b. 2D generated (nano) micro-patterns onto a GeSbTe film using a laser fluence of 1mJ/cm^2 and 4.74 μm diameter SiO_2 microspheres

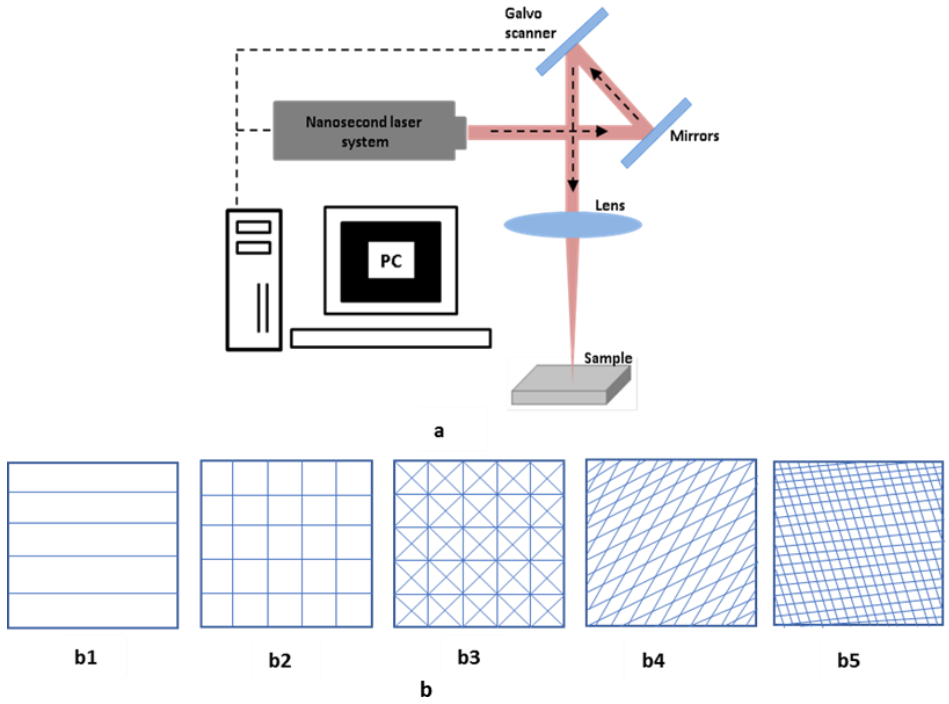

Fig. 1 (a) Experimental set up and (b) scanning directions with: (b1) one direction scanning, (b2) two directions scanning, (b3) four directions scanning, (b4) two directions with 30° & 60° scanning and (b5) two directions with 10° & 130° scanning

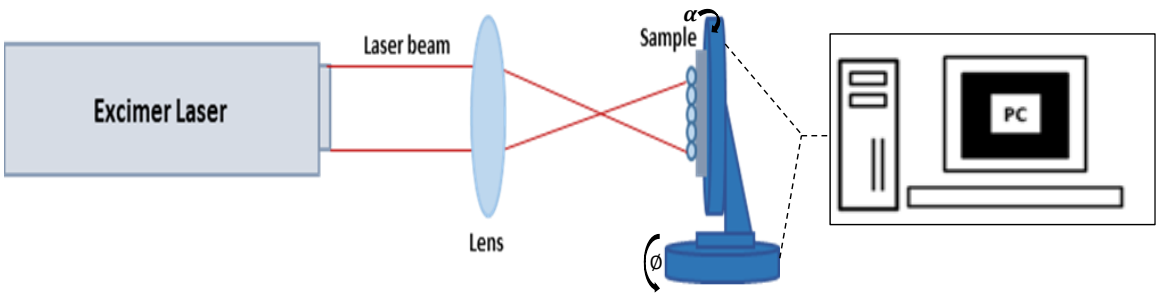

Fig.2 Experimental set up of surface texturing using particle lens array

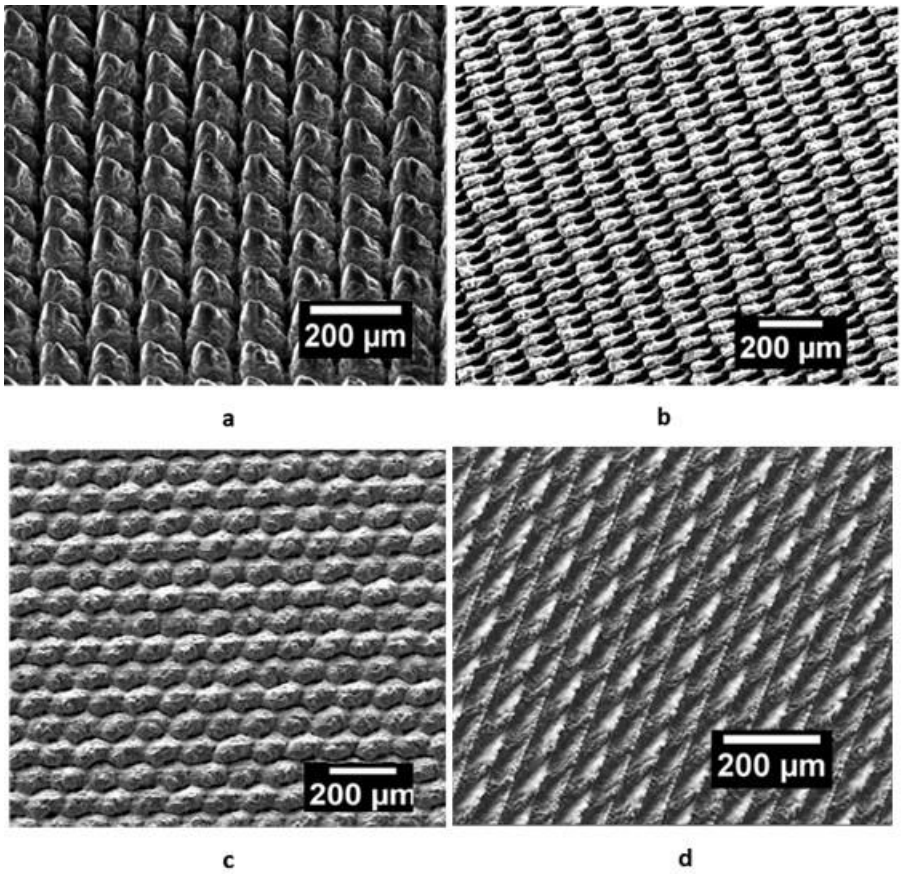

Fig. 3 Effect of the scanning direction on the microstructure morphology: (a) conical, (b) micro-pores, (c) beehive and (d) diamond-like structures.

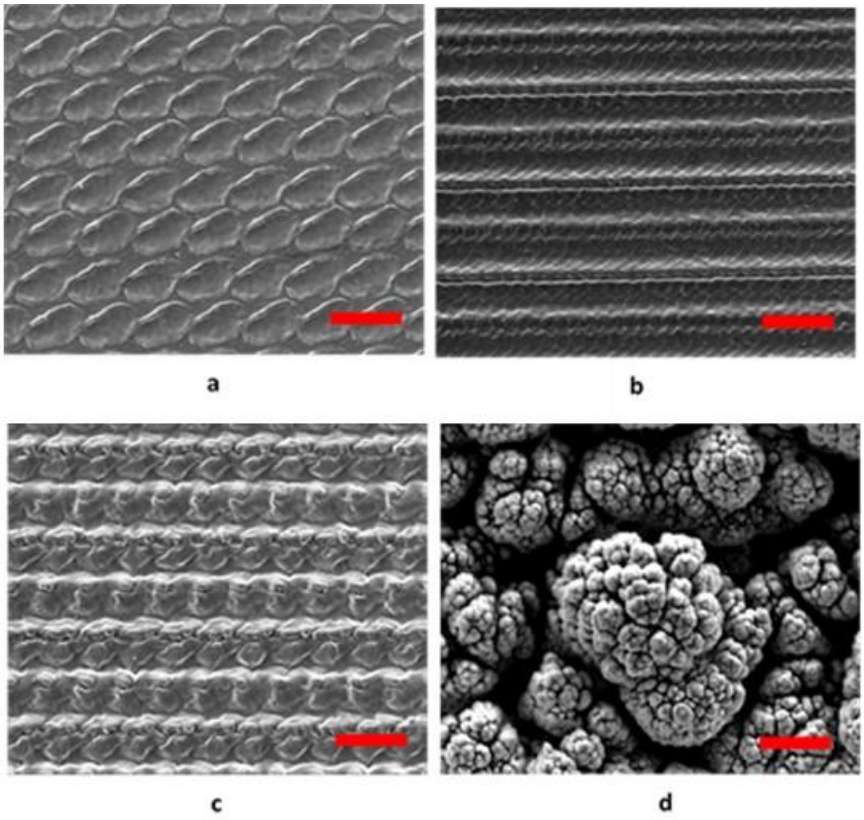

Fig. 4 Effect of scanning speed on the microstructure morphology using: (a) 2000 mm/s, (b) 500 mm/s, (c) 100 mm/s and (d) 1 mm/s. Scale bar is 200 μm

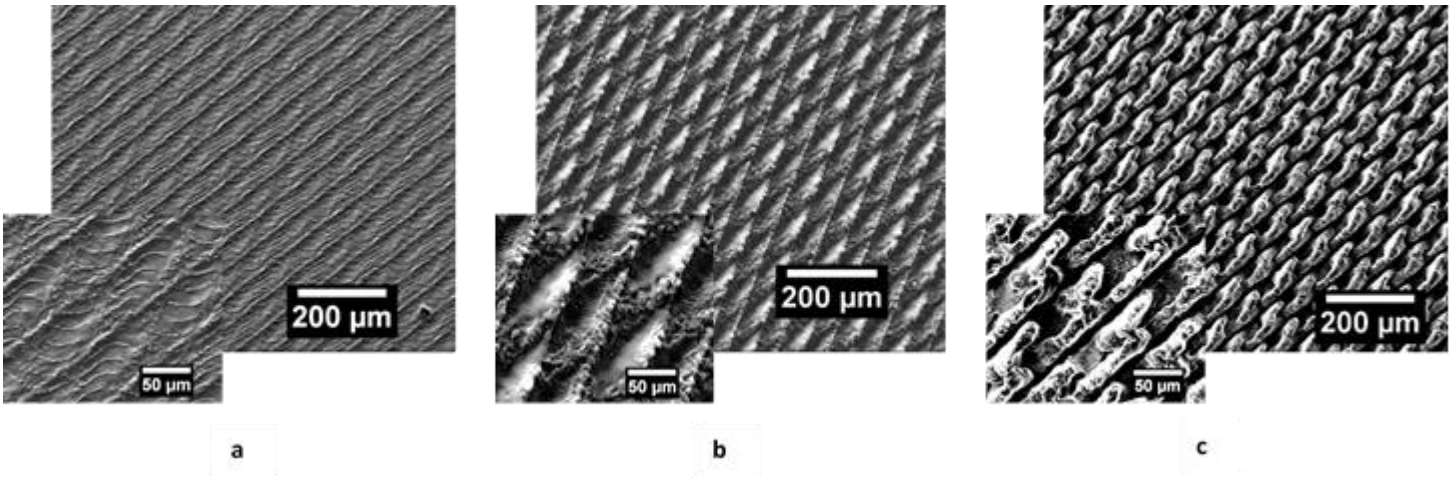

Fig. 5 Effect of laser fluence on the microstructure morphology using: (a) 0.9 J/cm², (b) 3.9 J/cm², and (c) 9.8 J/cm²

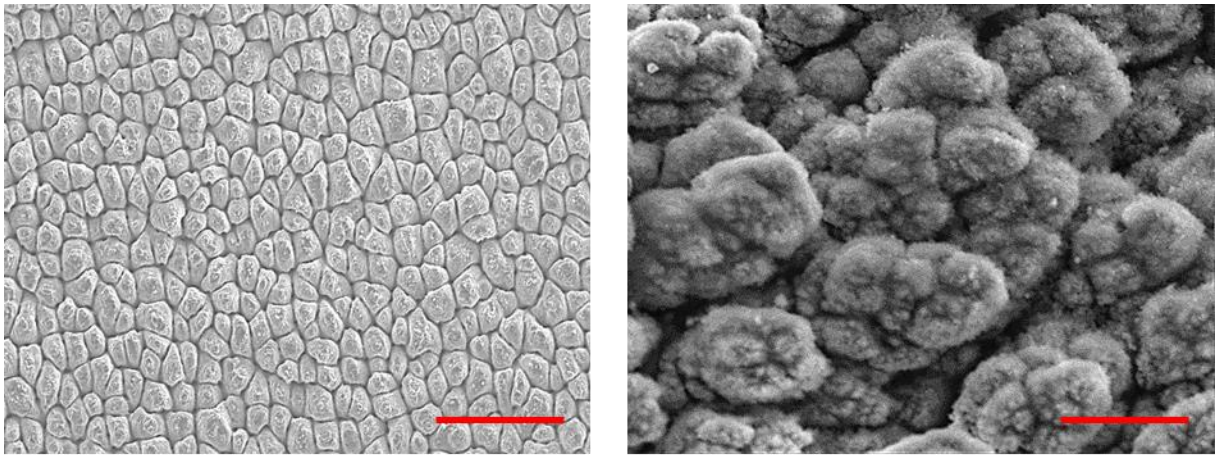

Fig. 6 The microstructure morphology generated in: (a) water, and (b) air, the scale bar is 50 μm

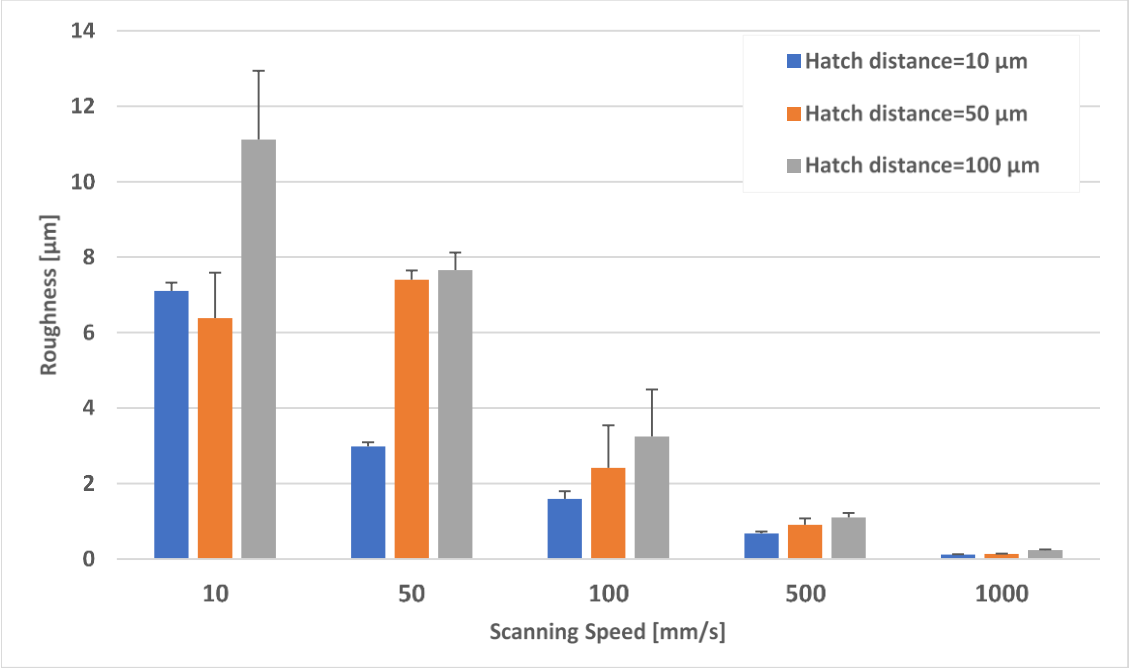

Fig. 7 The surface roughness measurements of laser treated surfaces

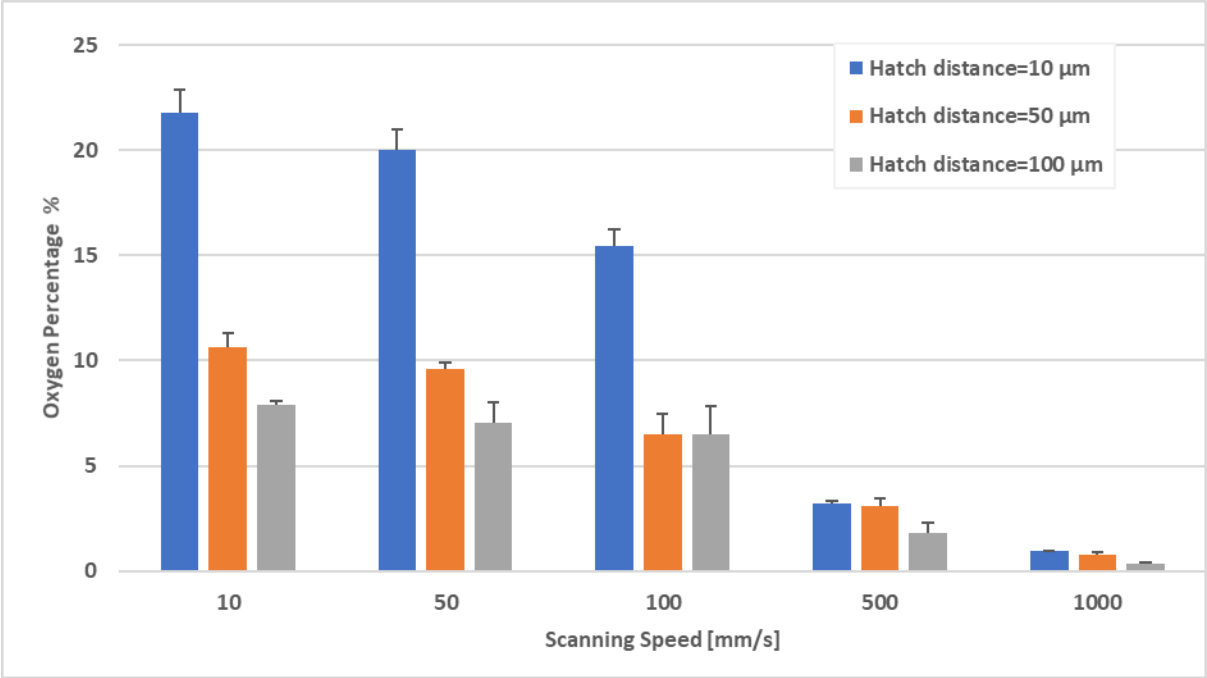

Fig. 8 The surface oxygen contents measurements of laser treated surfaces

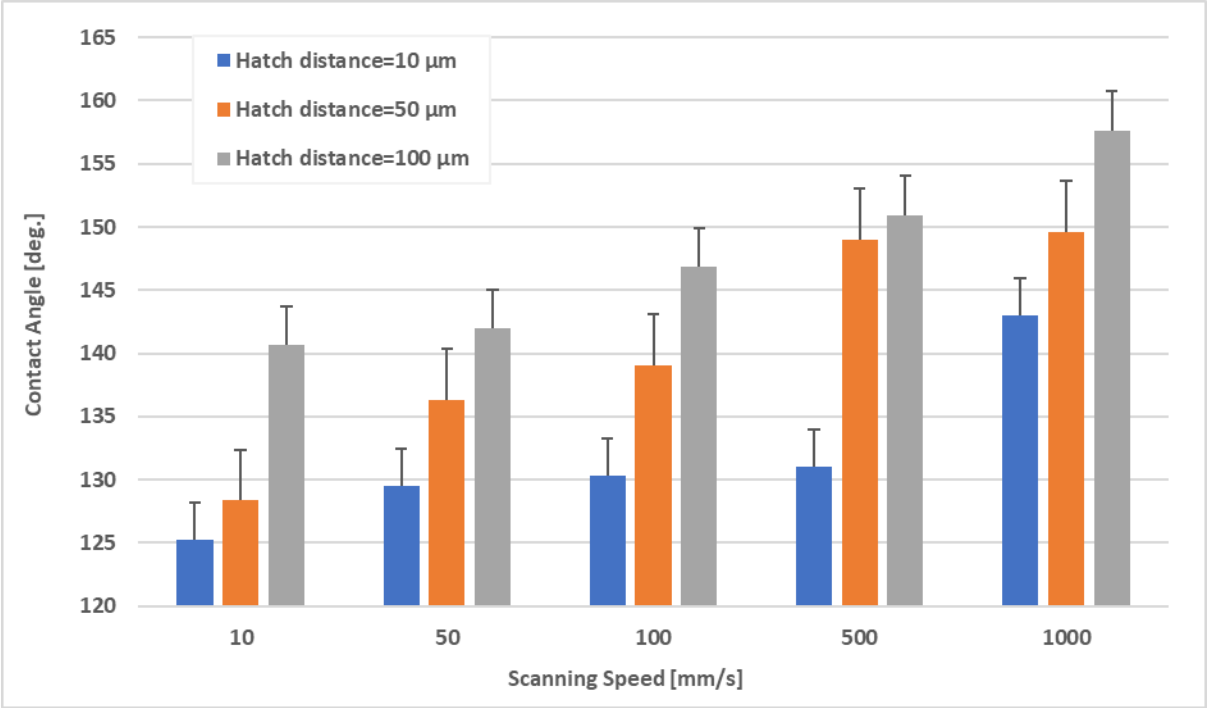

Fig. 9 The contact angle measurements of laser treated surfaces

689

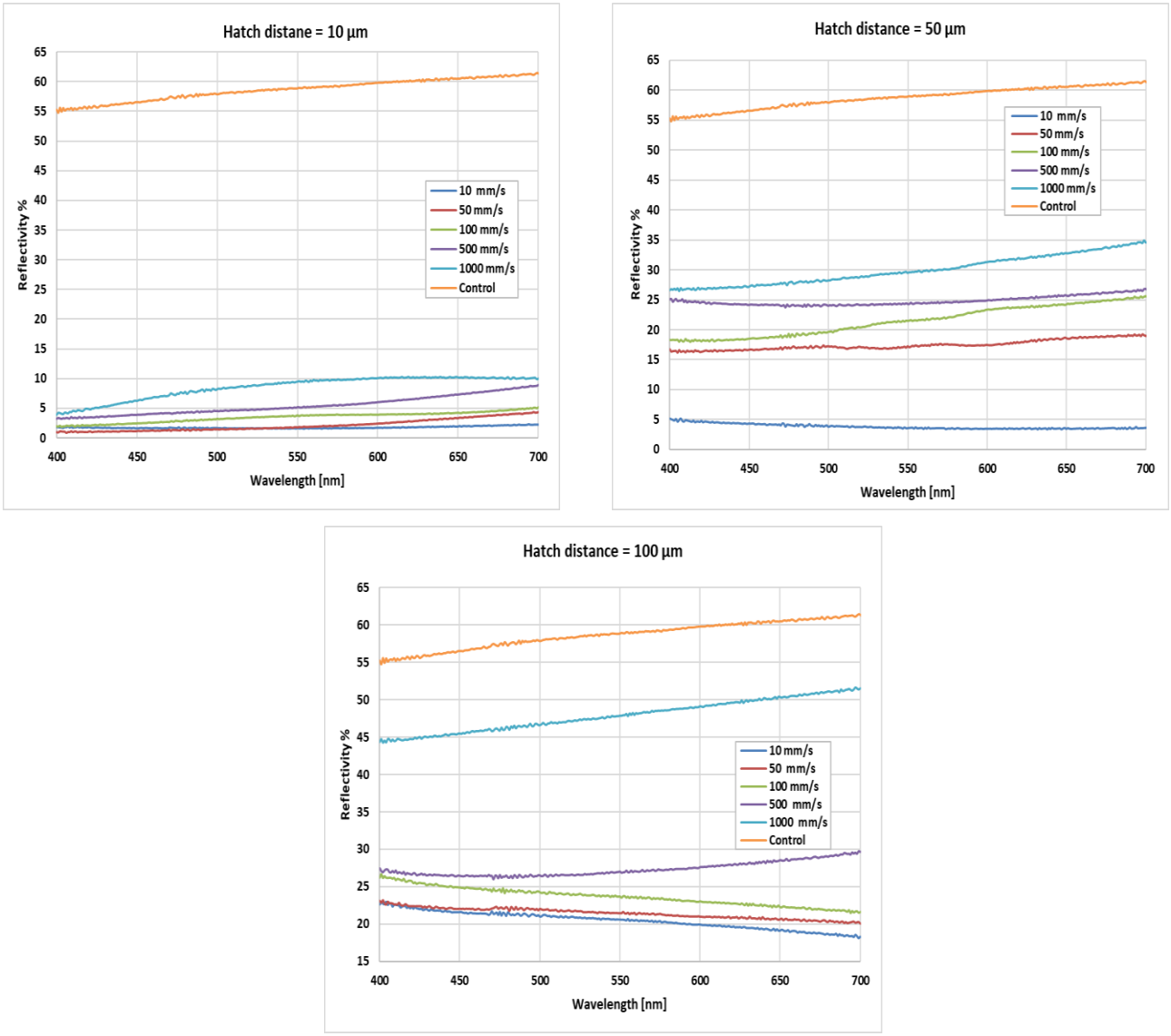

690

691 Fig. 10 The surface reflectivity measurements of laser treated surfaces

692

693

694

695

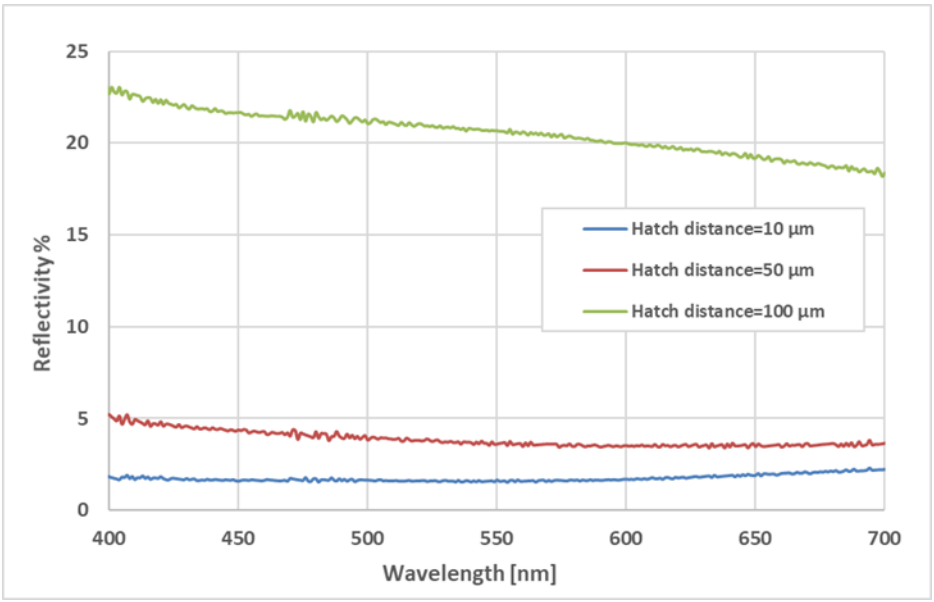

Fig. 11 The surface reflectivity measurements as a function of changing hatch distances at a scanning speed of 10 mm/s

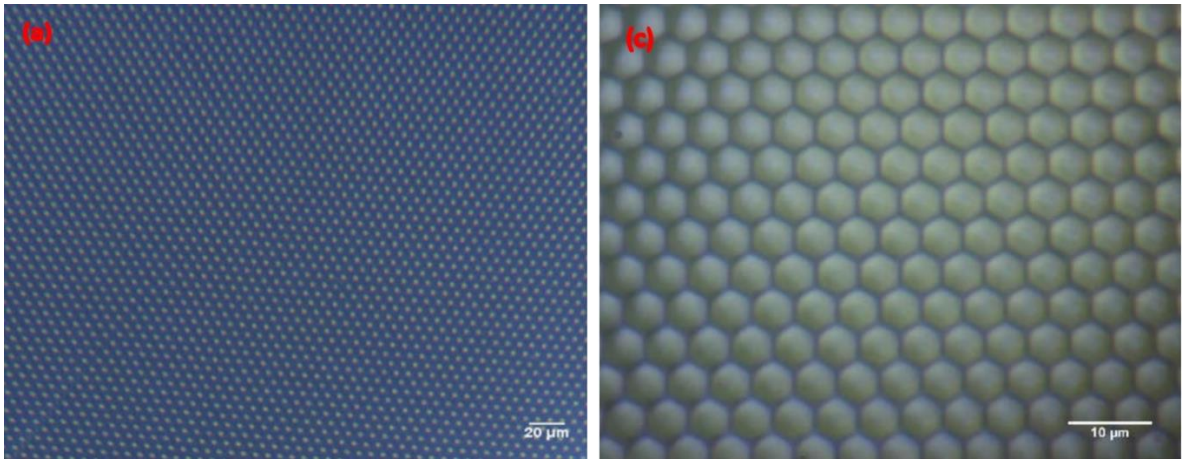

Fig. 12 Optical microscope image of a uniform layer of SiO_2 microsphere using: (a) 10X magnification and (c) 20X magnification

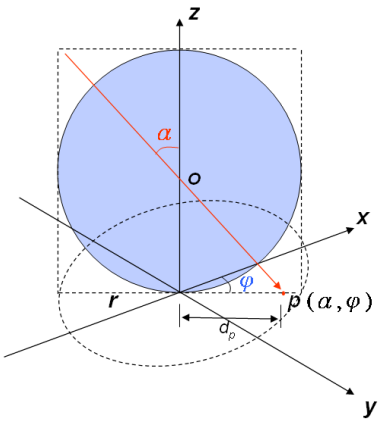

Fig. 13 Schematic diagram of geometric algorithm between the position of spot p, incident angle α and sample rotating angle ϕ

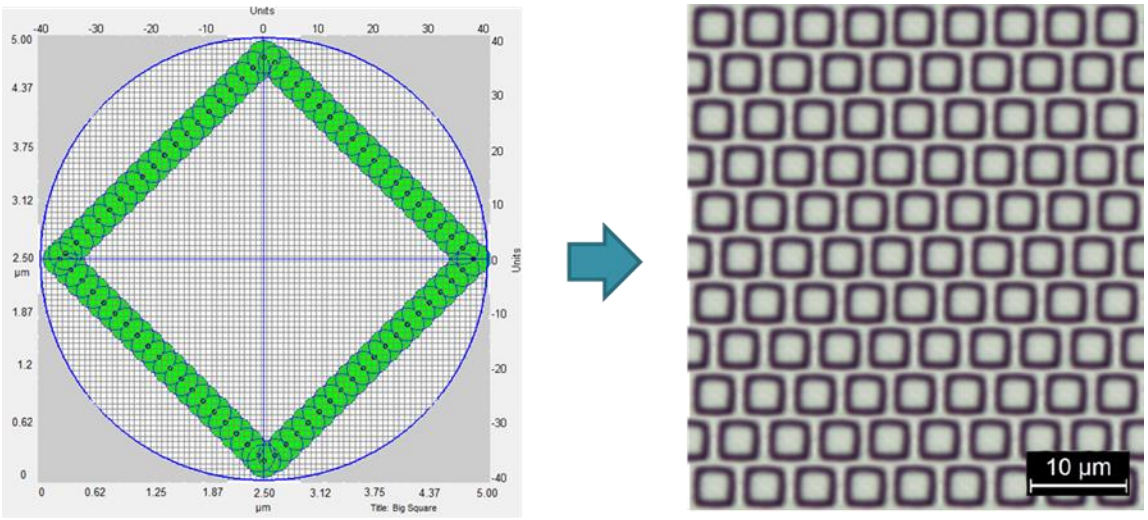

Fig. 14 a. Matlab® software interface; b. 2D generated square micro-patterns onto a GeSbTe film using a laser fluence of 1 mJ/cm^2 and 4.74 µm diameter SiO_2 microspheres

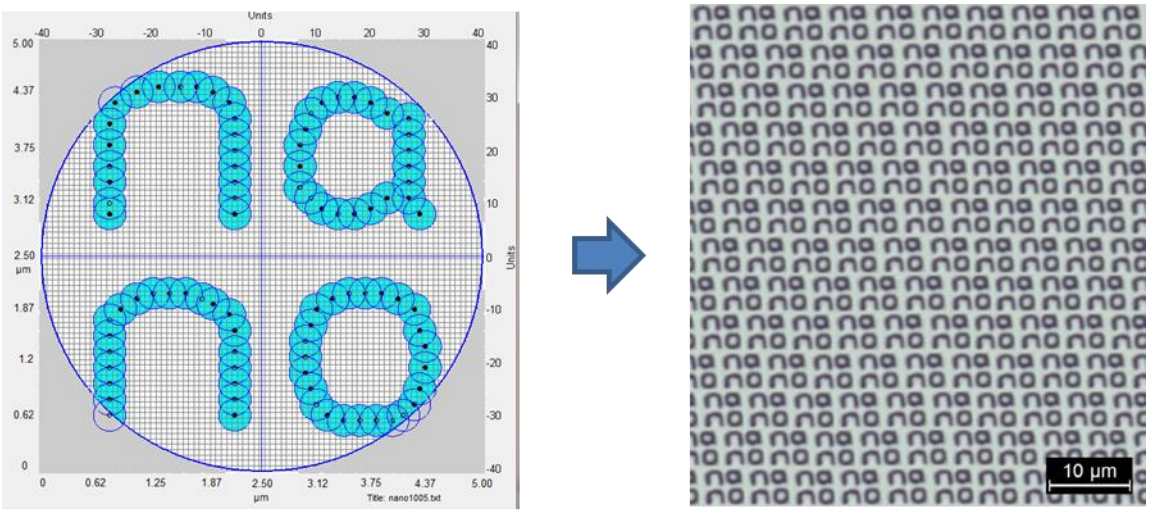

Fig. 15 a. Matlab® software interface; b. 2D generated (nano) micro-patterns onto a GeSbTe film using a laser fluence of 1 mJ/cm^2 and 4.74 µm diameter SiO_2 microspheres

770 **Table Caption List**
771

Table 1 The used nanosecond laser parameters for texturing the stainless steel

Table 2 Laser parameters for inducing different surface textures using Excimer laser

772

773

774

775

776

777

778

779

780

781

782

783

784

785

786

787

788

789

Table 1 The used nanosecond laser parameters for texturing the stainless steel

Laser parameters	**Nanosecond Laser (Nd:YVO_4)**
Wavelength [nm]	532
Pulse duration	7 ns
Pulse repetition frequency [kHz]	30
Focused diameter [µm]	55
Fluence [J/cm²]	0.9, 3.9 and 9.26
Speed [mm/s]	1, 10, 50, 100, 500, 1000 and 2000
Hatch distance [µm]	10, 50 and 100
Focal length [mm]	245

Table 2 Laser parameters for inducing different surface textures using Excimer laser

Laser parameters	**Nanosecond Laser (Excimer Laser)**
Wavelength [nm]	248
Pulse duration [ns]	15
Pulse repetition frequency [Hz]	1
Focused beam size [mm]	10 × 10
Fluence [mJ/cm²]	1